Pulse compression in parametric amplification

Xuan Luo, Ning Hsu, Jens Biegert, Ladan Arissian and Jean-Claude Diels

University of New Mexico,
Department of Physics & Astronomy,
Albuquerque, NM 87131, U.S.A.

to appear in
Wiley Encyclopedia of RF and Microwave Engineering

April 30, 2017

Contents

1 Introduction

The main objective of this Chapter is to provide the fundamental theoretical and numerical tools to design ultrashort pulse manipulation through optical parametric amplification. By manipulation it is understood a number of application present and future. Some examples of application (not all of them will be covered in this chapter) are:

- Pulse compression in second harmonic generation
- Pulse compression and amplification down to a few optical cycles through difference frequency generation
- Generation of giant chirp in frequency mixing for pulse broadening or compression by further propagation in dispersive media
- Generation of mid- and long wavelength infrared ultrashort pulses
- Pulse characterization by cascaded nonlinearity
- Autostabilization of synchronously pumped Optical Parametric Oscillators (OPO's)
- Design of Fourier Optical Parametric Amplifiers (FOPA).

A prerequisite for pulse compression is clearly the fact that the processes involved have to respond instantaneously on the time scale of the shortest optical pulse. Nonlinear crystals lend themselves nearly ideally to frequency conversion with ultrashort pulses because their nonlinearity is electronic and non-resonant. There appears to be no limit in the palette of frequencies that can be generated through nonlinear optics, from dc (optical rectification) to infrared (difference frequency generation and optical parametric generation and amplification), to visible, and to UV (sum frequency generation). The shorter the pulse, the higher the peak intensity for a given pulse energy (and thus the more efficient the nonlinear process). While from the microscopic point of view, the nonlinearity is electronic and non-resonant, from the macroscopic point of view the phase matched crystal acts as a resonant element, and there is a response time associated with the phase-matching bandwidth.

There is an insidious problem that complicates nonlinear optics with ultrashort pulses: the velocity of a wave packet is not the same as that of the individual waves. In second harmonic generation, even though the fundamental and second harmonic waves are "phase matched" (i.e., these waves propagate at the same wave velocity), the fundamental pulse propagates at a different velocity (in general faster) than the second harmonic pulse. This effect, generally labeled group velocity dispersion, appears to be the nemesis of most frequency mixing schemes. In general, because of group velocity dispersion, the second harmonic will propagate more slowly than the fundamental that feeds it. Therefore, the nonlinear interaction between two pulses of duration τ at frequencies ω_1 and ω_2 is limited to the walk-off distance $L = \tau/({v_{g1}}^{-1} - {v_{g2}}^{-1})$, where v_{g1} and v_{g2} are the group velocities at their respective wavelengths. For instance, in type I interaction, the second harmonic of 800 nm radiation in BBO ($\beta - BaB_2O_4$) is delayed with respect to the fundamental by 194 fs/mm. Therefore, very thin (< 1 mm) crystals are generally selected for all nonlinear mixing processes involving femtosecond pulses. It has been shown however that group velocity dispersion, combined with amplitude modulation associated with the depletion of the fundamental waves, can lead to efficient pulse compression [1, 2]. Small amounts of compression were first demonstrated with subpicosecond pulses [3, 4]. Subsequently, pulse compression through second harmonic generation in very long (5-6 cm) KDP (KH_2PO_4) and KD*P (KD_2PO_4) crystals was predicted [2] and demonstrated [5]. It should be noted that a similar compression mechanism has been investigated in synchronously pumped optical parametric oscillators [6, 7, 8, 9].

2 Equations for wave mixing

In most books of nonlinear optics [10, 11] parametric processes are treated in time domain, mainly because the nonlinear polarization is proportional to the product in time domain) of the optical electric fields. This representation is adequate for continuous fields at discrete frequencies. Coupled equations are generally written for the temporal and spatial evolution of the fields at different frequencies, involving frequency dependent parameters such as the index of refraction. This is not a proper approach for ultrashort pulses, since it is mixing time and frequency in the evolution equations. For broadband radiation, each component propagates at a different phase velocity. In order to fully account to all order for the dispersion of the various parameters (linear and nonlinear index of refraction), we establish a set of interaction equations in the frequency domain. The nonlinear interaction will be modeled here for optical parametric amplification with a crystal either phase matched, or quasi phase matched for the difference frequency generation (DFG) $\omega_s = \omega_p - \omega_i$ (where ω_p is the pump frequency, ω_i for "idler" in the case of an OPO, and ω_s the difference signal). Even though other nonlinear processes are phase-mismatched, they have a non-negligible impact on the phase matched process of parametric amplification, mostly through phase coupling. These phase mismatched processes are second harmonics generation (SHG) and sum frequency generation (SFG), as sketched in the diagram of Fig. 1. The frequencies involved are the second harmonic of the pump at $\omega_2 = 2\omega_p$, the sum frequency of pump and signal at $\omega_3 = \omega_s + \omega_p$, the second harmonic of the signal at $\omega_4 = 2\omega_s$, and the sum frequency of pump and idler at $\omega_5 = \omega_i + \omega_p$. For sake of clarity, and better understanding of the physics involved, we will consider only the most intense fields, ignoring the last two frequencies ω_4 and ω_5 which involve weaker fields.

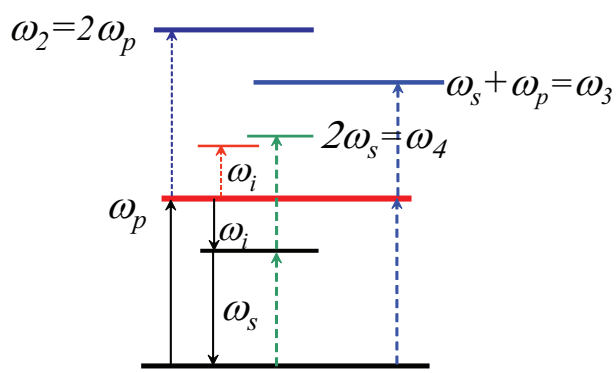

Figure 1: Diagram illustrated the different sum and difference frequency processes involved in parametric amplification. Only the difference process $\omega_p = \omega_s + \omega_i$ is phase matched.

2.1 Interaction equations

Maxwell's propagation equations for the five fields, written in the frequency domain, can be separated within the reasonable assumption that the Fourier spectra of the pulses at the five frequencies do not overlap. This derivation was first introduced to describe phase matched second harmonic generation with birefringent crystals [12, 13]. The equations are presented in the plane wave approximation (no transverse spatial dependence). Maxwell's propagation equations in the frequency domain is written as:

$$\left[\frac{\partial^2}{\partial z^2} + \Omega^2 \mu\epsilon(\Omega)\right] \tilde{\mathbf{E}}(\Omega, z) = -\mu_0 \Omega^2 \tilde{\mathbf{P}}^{NL}(\Omega, z). \tag{1}$$

The second order nonlinear polarization is made of products of pairs of fields, *in the time domain* $P_i^{NL}(t,z) = \epsilon_0 \left[\sum_j \chi^{(2)}_{j+k} E_j E_k + \sum_\ell \chi^{(2)}_{j-k} E_j E_k^*\right]$ where the first terms are sum frequency (SF) process, and the second terms difference frequency (DF). In the case of aperiodically poled crystals, the optical axis is chosen along

the direction of polarization, and the nonlinear susceptibility is represented by a Fourier series with the fundamental grating period being k_g: $\chi = \sum_m \chi_m^{(2)} \sin(mk_g z)$. When the crystal is *periodically* poled (PPLN), only the odd m coefficients exist, with amplitudes inversely proportional to m. Substituting for each field, in the frequency domain, $E_i(\Omega, z) = \tilde{\mathcal{E}}_i(\Omega, z) \exp[-ik_i(\Omega)z]$, in Eq. (1), we find that, for a PPLN, the nonlinear interaction equations can be written in the simple form:

$$\begin{aligned} \frac{\partial \tilde{\mathcal{E}}_i(\Omega)}{\partial z} &= -\sum_{m=1,3,5,\cdot} \frac{ik_i(\Omega)}{4n_i^2} \chi_{jk}^{(2)} \left\{ \left[\tilde{\mathcal{E}}_j(\Omega, z) e^{-ik_j(\Omega)z} \right] \star \left[\tilde{\mathcal{E}}_k(\Omega, z) e^{-ik_k(\Omega)z} \right] \right\} e^{ik_i z} \frac{\sin mk_g z}{m} \\ &\quad + \frac{i}{2k_i} \frac{\partial^2 \tilde{\mathcal{E}}(\Omega, z)}{\partial z^2}, \end{aligned} \tag{2}$$

where the symbol "$\star$" represents a convolution for DF, and a correlation for SF, and $k_g = 2\pi/\Lambda$ where Λ is the period of the PPLN grating. In the case where the nonlinear interaction is in an angle tuned crystal, the set of equations simplifies to:

$$\begin{aligned} \frac{\partial \tilde{\mathcal{E}}_i(\Omega)}{\partial z} &= -\frac{ik_i(\Omega)}{4n_i^2} \chi_{jk}^{(2)} \left\{ \left[\tilde{\mathcal{E}}_j(\Omega, z) e^{-ik_j(\Omega)z} \right] \star \left[\tilde{\mathcal{E}}_k(\Omega, z) e^{-ik_k(\Omega)z} \right] \right\} e^{ik_i z} \\ &\quad + \frac{i}{2k_i} \frac{\partial^2 \tilde{\mathcal{E}}(\Omega, z)}{\partial z^2}, \end{aligned} \tag{3}$$

The set of equations (2) or (3) describe the propagation of the fields in the frequency domain. In the examples presented in the following applications sections, they are integrated along the propagation direction, using a Butcher predictor-corrector method [14], to calculate the Fourier transforms of the fields $\tilde{\mathcal{E}}_i(\Omega, d)$ after propagation through the thickness d of the crystal.

Phase variations in the set of Eqs. (2) are generally too fast for practical numerical integration. This problem is solved by writing the electric fields in a frame of reference moving at the group velocity of one of the waves. The spectral fields are written in coordinates centered at the average frequency of each pulse. Details of the various changes of variables and functions for numerical convenience are given in refs. [13, 15, 16].

Equations (2) or (3) describe the nonlinear interaction accurately to all orders without any approximations. It would be desirable, however, to neglect the second derivatives of the electric fields in order to simplify the equations and to speed up the already involved numerics. We have calculated that in a worst case scenarios of the generation of a 3 fs second harmonic pulse, the maximum value for $\partial^2\tilde{\mathcal{E}}/\partial z^2$ is 200 times smaller than $2k\,\partial\tilde{\mathcal{E}}/\partial z$, and can therefore be neglected. Hence, we conclude that for the pulse durations under investigation, the reduction to a system of first order differential equations suffices.

When relevant, the effect of the non resonant-nonlinear index of refraction $n_2 I(t)$ (where $I(t)$ is the pulse intensity) can be calculated by a split step method. At steps intervals Δz, the fields are inverse Fourier transformed in the time domain to give $\tilde{\mathcal{E}}(t)$, multiplied by the phase factor $\exp\{i[2\pi n_2 I(t)\Delta z/\lambda]\}$ before being transformed back in the frequency domain.

3 Pulse compression from ps to fs

Most sources of high power short pulse sources start from a fs pulse source such as a mode-locked Ti:sapphire laser [17, 18], broaden the pulse by several orders of magnitude through negative dispersion, amplify linearly in an amplifier chain before re-compressing through positive dispersion. An alternative to these complex and delicate systems is to use more efficient longer pulse laser systems such as Nd:YAG (the workhorse of the industry) and compress the pulses by nonlinear methods. One method used successfully for pulse energies over 1 J is stimulated Brillouin scattering. Frequency doubled Nd:YAG lasers pulse of more than 2J energy

were compressed from 10 ns down to 200 ps with minimum loss of energy [19, 20, 21]. Such systems however are not compact, since the length of Brillouin medium required should be equal to the pulse length (≈ 10 m for 10 ns pulses in the case of the references cited). Another option is to use sum frequency or second harmonic generation as demonstrated in this section.

Lets us consider second harmonic generation of two interacting fundamental waves with orthogonal polarizations (type II). Furthermore, assume the second harmonic the group velocity (an extraordinary wave) to be intermediate between that of the ordinary o and extraordinary e fundamental waves. The second harmonic e wave is being generated by the nonlinear polarization $P_{e,NL} = \epsilon_0 \chi^{(2)} E_o E_e$, where $E_j = \mathcal{E}_j \exp i(\omega t - k_j z)$ ($j = o, e$) are the electric fields of the ordinary and extraordinary fundamental waves and $\chi^{(2)}$ is the second-order nonlinear susceptibility. The wave vectors of the ordinary and extraordinary fundamental waves are $k_o = \omega n_o(\omega)/c$ and $k_e = \omega n_e(\omega)/c$ and for the second harmonic wave $k_2 = \omega n_2(\omega_2)/c$, respectively; $n_o(\omega)$, $n_e(\omega)$ and $n_2(\omega_2)$ are the refractive indexes of the nonlinear crystal. This nonlinear polarization generates a second harmonic field as an extraordinary wave $E_2 = \mathcal{E}_2 \exp i(\omega_2 t - k_2 z)$ at the frequency $\omega_2 = 2\omega$. The propagating second harmonic will remain in phase with the second harmonic generated at any point z in the crystal, if momentum conservation ("phase matching") is satisfied:

$$k_2 = k_o + k_e. \tag{4}$$

This phase matching condition is satisfied if the crystal orientation is chosen such that:

$$n_2 = \frac{n_o + n_e}{2}. \tag{5}$$

The phase matching condition implies that the *phase velocities* are matched. After a propagation length L through the crystal, the phase delay of the second harmonic $L/v_{p,2}$ is equal to the sum of the phase delay of the two fundamentals $L/v_{p,o} + L/v_{p,e}$. The phase velocities are defined as:

$$v_{p,2} = \frac{c}{n_e(\omega_2)} \qquad v_{p,o} = \frac{c}{n_o(\omega)} \qquad v_{p,e} = \frac{c}{n_e(\omega)}. \tag{6}$$

The fact that the waves remain in phase does not necessarily imply that *pulses* reach simultaneously the end of the crystal. The three wave packets propagate at the *group velocities* given by:

$$\begin{aligned} \frac{1}{v_{g,2}} &= \frac{1}{c}\left[n_e(\omega_2) - \lambda \left.\frac{dn_e}{d\lambda}\right|_{\omega_2}\right] \\ \frac{1}{v_{g,o}} &= \frac{1}{c}\left[n_o(\omega) - \lambda \left.\frac{dn_o}{d\lambda}\right|_{\omega}\right] \\ \frac{1}{v_{g,e}} &= \frac{1}{c}\left[n_e(\omega) - \lambda \left.\frac{dn_e}{d\lambda}\right|_{\omega}\right]. \end{aligned} \tag{7}$$

It is important to remember that these definitions of "*group velocity*" apply only to the *distortion-less*" propagation of pulses in a pure *dielectric*. Frequency dependent gain or absorption my modify considerably the velocity at which the pulse envelope propagates, as demonstrated in the case of synchronously pumped optical parametric oscillators (OPO) in Section 6 of this chapter. An example of a dramatic difference between the definition of Eqs. (7) and the real pulse envelope velocity in a cavity is given in references [22, 23]).

If a fundamental pulse with an e and o component enters the crystal, it will generate a second harmonic pulse which will propagate at a different group velocity than either component of the fundamental. We have required that the velocity of the second harmonic is intermediate between that of the two fundamentals. Let us now consider the case where the fundamental e wave enters the crystal *delayed* with respect to the fundamental o wave. A second harmonic will be generated at the temporal overlap between the two pulses, as sketched in Fig. 2(a). In a frame of reference moving at the group velocity of the second harmonic, the two fundamental pulses will travel towards each other (since the faster e wave has been delayed). After some propagation distance, the overlap of the fundamentals increases, and so does the second harmonic (Fig. 2(b)).

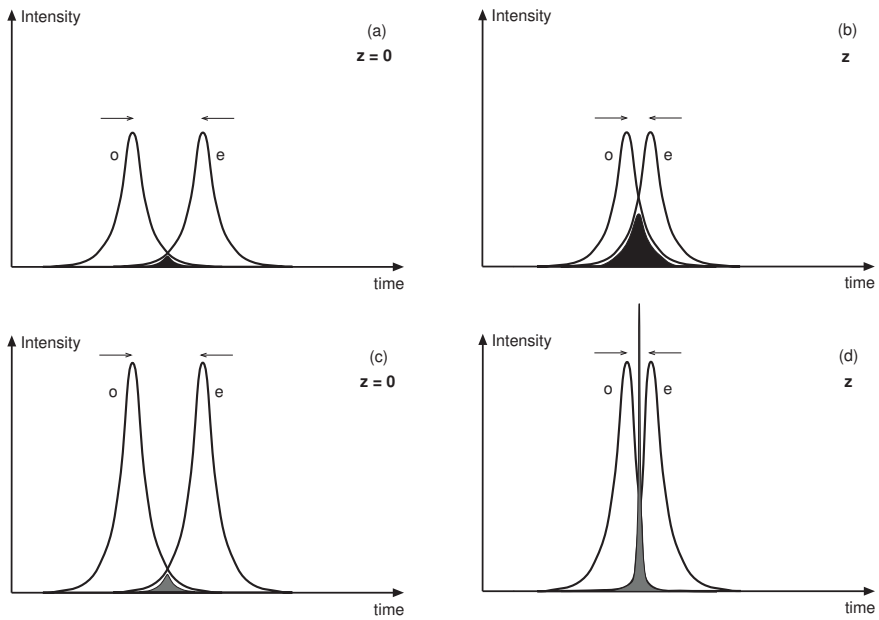

Figure 2: The three pulses are represented in a temporal frame of reference moving with the group velocity of the second harmonic. Initially, at $z = 0$, the fundamental e is delayed with respect to the fundamental o wave (Figs. (a) and (c)). For low input energies (a), the second harmonic will be broadened as the two fundamental pulses move into each other (b). For sufficiently high input energies (c), the overlap between the two fundamentals remains small because they are depleted by the up-conversion process, and the second harmonic pulse remains short (d).

However, if the fundamental pulses are sufficiently intense as sketched in Figs. 2(c) and (d), the growth of the second harmonic may be so fast as to deplete the fundamentals. As a result, the spatial overlap of the two fundamentals remains small, as they move into each other (Fig. 2(d)). Crude order of magnitude estimates of the power required can be made by considering square fundamental pulses (temporal profile). Let us assume first that the group velocity of the second harmonic is exactly the average of the group velocities of the extraordinary and ordinary fundamentals. If, as in Fig. 2 (a), the two fundamental pulses are given a pre-delay, they will move across each other, in a frame of reference moving with the second harmonic, as they propagate through the crystal. One expects also that the second harmonic pulse will be even longer than the fundamental. At perfect phase matching, the second harmonic generated after a distance z is given by [24]:

$$\mathcal{E}_2(z) = \mathcal{E}(0)\tanh\frac{z}{L_{sh}} \tag{8}$$

where, at $z = 0$, $\mathcal{E}_o = \mathcal{E}_e = \mathcal{E}$, and the characteristic distance L_{sh} is given by:

$$\frac{1}{L_{sh}} = \frac{\omega\chi^{(2)}}{n_2 c}\mathcal{E}. \tag{9}$$

For optimum production of a second harmonic pulse of duration τ_{ov}, the fundamental pulses should move into each other by an overlap time τ_{ov}, over the characteristic distance L_{sh}. The condition

$$\tau_{ov} = \frac{n_2 c}{\omega\chi^{(2)}\mathcal{E}}\left(\frac{1}{v_{g,e}} - \frac{1}{v_{g,o}}\right) \tag{10}$$

leads to an optimum intensity $I_0 = W_0/\tau_{ov}$ (where W_0 is the pulse energy density over the overlap time) for the fundamental pulses. The intensity I_0 of the fundamental square pulses is given by:

$$I_{o,e} = \frac{\epsilon_0 c n_{o,e}\mathcal{E}^2}{2} = \frac{\epsilon_0 c^3 n_{o,e} n_2^2}{2(\omega\chi^{(2)}\tau_{ov})^2}\left(\frac{1}{v_{g,e}} - \frac{1}{v_{g,o}}\right)^2. \tag{11}$$

The following simulations are based on second harmonic generation in KDP, where the full Sellmeier formulae have been used in the definition of the various k vectors that appear in the wave equations. As a result, our model takes into account *all* group velocity dispersion effects as they affect the pulse propagation and the pulse conversion process. In agreement with the simple considerations at the beginning of this section, the width of the generated second harmonic is determined by the depletion of the two fundamentals moving into each other. The situation is much more complex when the full frequency dependence of the k vectors is taken into account. Perfect phase matching exists only for a single frequency component. Because of the frequency dependence of the wave vectors, there will be some transfer of energy back from the second harmonic to the fundamental. Figure 3 illustrates the propagation and harmonic generation of two fundamental pulses with a

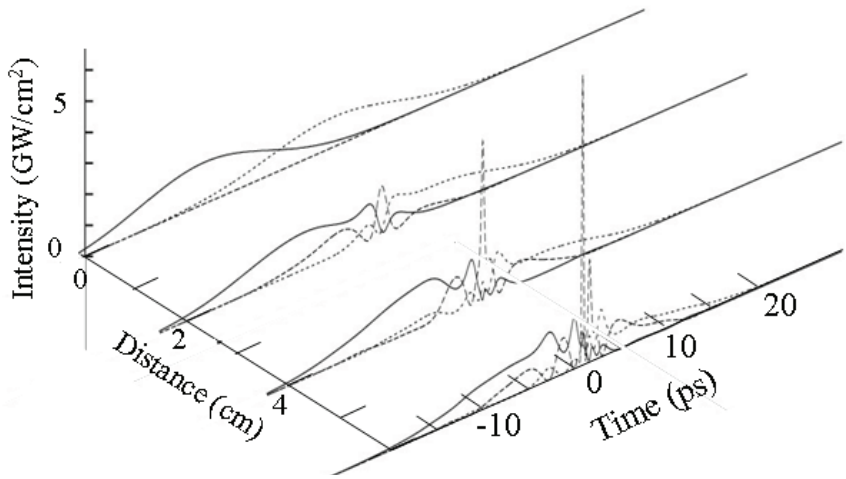

Figure 3: Three dimensional representation of the propagation of the fundamental and the second harmonic pulses. Solid and dotted lines: the fundamental pulses counterpropagating in a retarded frame at the group velocity of the second harmonic. Dashed line: the generated (and compressed) second harmonic peaking between the fundamentals.

Gaussian temporal profile. The fundamental ordinary and extraordinary waves have respectively intensities of 1.4 and 1 GW/cm^2, with the extraordinary wave being pre-delayed by 14 ps with respect to the ordinary wave. A three dimensional representation of the propagation of the intensities of the three waves inside a 6 cm long KDP crystal is shown in Fig. 3.

These calculations have been verified experimentally, using as a source an active-passive mode-locked Nd:YAG laser controlled by passive negative feedback with successive amplifier stages [6]. The system was adjusted to yield 14 ps pulses with pulse energies up to 150 mJ. The linearly polarized output beam passes through a half-wave plate which rotates its plane of polarization by 45°. The beam is then separated into two components by a polarizing beam splitter, and each component is being given a relative delay before being recombined at a second polarizing beam splitter. The rotation of the wave plate enables one to control the ratio between the energies of both beams. The recombined pulses are sent as e and o waves into the second harmonic generating crystal (6 cm long KDP). A portion of uniform intensity at the beam center is selected by a 9 mm apodized aperture positioned just before the crystal, giving a better than 95 % top-hat transverse beam profile. The total power density of the 1.06 μm beam incident on the 6 cm long KDP crystal was 2.6 GW/cm^2. The fundamental e beam was given a predelay of 10.5 ps with respect to the o wave. The intensity of the o pulse was 1.3 times that of the e pulse. The conversion efficiency was 14%. The width of the autocorrelation curve of the (green) compressed pulse is 480 fs, which corresponds to a sech^2 pulse of 309 fs duration. The compression factor is thus 45. Details of the experiment can be found in reference [25].

4 Generation of giant phase modulation for pulse compression

The most common method of compressing pulses is to apply a phase modulation in the time domain, followed by dispersion [15]. Phase modulation in the time domain is done through the Kerr effect for ultrashort pulses, which results in a nonlinear index $\Delta n = n_2 I$ proportional to the intensity I of a pulse. The nonlinear index being generally positive, the resulting frequency modulation is an upchirp in the central part of the pulse. In order to compress the modulated pulse, a negative dispersion has to be applied, which implies an arrangement of prisms or gratings in the visible. Because of the spatial dependence of the intensity, self-focusing is associated with the positive nonlinear index, resulting in laser damage in bulk solid state media. An elegant solution to this problem was devised by creating a sequence of glass plates, of such thickness that Kerr phase modulation and dispersion results in an incremental compression, but thin enough to prevent beam collapse. The spacing between the plates is such that diffraction between plates compensates the Kerr lensing occurring within each plate [26, 27]. This technique has been used successfully to compress ultrashort pulses down to a few optical cycles. Another approach is to create phase modulation by using cascading nonlinearity. H. J. Bakker et al [28, 29] did an analytical and numerical study on the phase modulation induced by second-order nonlinear process, in which they found that the phase modulation can be represented by an effective nonlinear index n_2^{eff} function of the phase-mismatch, pulse intensity, initial phase, and group velocity mismatch (GVM) between interacting waves. An experimental measurement of n_2^{eff} by R. DeSalvo et al [30] on a KTP crystal showed the sign of n_2^{eff} to be reversible by changing the sign of the phase mismatch ΔkL. The property that n_2^{eff} can be engineered to have the desired sign and large values has an important impact on the field of pulse compression. It is often desirable to apply a *negative* phase modulation to a short pulse, in order to enact pulse compression in a positively dispersive medium. This is the case for instance when launching intense short wavelength pulses in the atmosphere, with the aim of creating remotely a filament, for instance for spectroscopy at a large standoff distance. Negative n_2^{eff} has the additional advantage that a large modulation can be imparted on a pulse without inducing catastrophic collapse through self-focusing.

As an example, let us consider sum frequency generation (SFG) of a 25 ps pulses at 1064 nm and 532 nm, resulting in a sum frequency at the wavelength of 355 nm. In the simulated experiment, these two fundamental pulses are sent collimated through a 5 cm KDP crystal with a slightly phase-mismatched angle to generate a spectral broadened 355 nm downchirped pulse.

Since the n_2^{eff} is strong only when the nonlinear conversion is close to phase-matching condition rather than at the perfect phase-matching point, the KDP crystal orientation has to be carefully considered and optimized. To estimate the phase-matching angle, the nonlinear conversion efficiency of a type I ($o + o \rightarrow e$) SFG as a function of KDP orientation is calculated using the Sellmeier equation as shown in Fig. 4(a). An optimum angle of 47.24 degree, equivalent to $\Delta kL = 0.32\pi$, is chosen to obtain maximum spectral broadening and downchirp on the 355 nm pulse. The initial conditions for the calculations presented in Fig. 4(b) are two co-propagating plane waves with Gaussian temporal profile of 25 ps duration and peak intensities of $I_{1064} = 20$ GW/cm^2 and $I_{532} = 20$ GW/cm^2. The simulations in Fig 4(b) show that a very large bandwidth increase can be obtained by cascaded nonlinearity in frequency mixing when the 355 nm is generated and propagated colinear with the two other wavelengths in the KDP crystal. The pulse spectrum is seen to be split in isolated components, that are still coherent with each others, since the generated 355 nm pulse in time maintains a 25 ps uniform bell shape.

A 3.5 ps compressed pulse as shown in Fig 4(c) is obtained by sending the spectrally broadened, down-chirped pulse into an optical element with a large quadratic dispersion. The transfer function of that optical element is defined as $\mathcal{T}(\Omega = \exp\{-i[\psi(\Omega)]\}$, and the quadratic dispersion is the second order derivative $d^2\psi/d\Omega^2$[15]. Figure 4 indicates that for a large positive dispersion of $\psi'' = 16.9$ ps^2 a seven-fold compression factor is obtained. The ripples of the pulse is the result of group velocity mismatch between 355 nm and 1064 nm and 532 nm. Further compression down to hundreds of fs is possible in multi-stages configuration [31]. A positive dispersion as large as tens of ps^2 can be easily achieved with a four grating arrangement similar

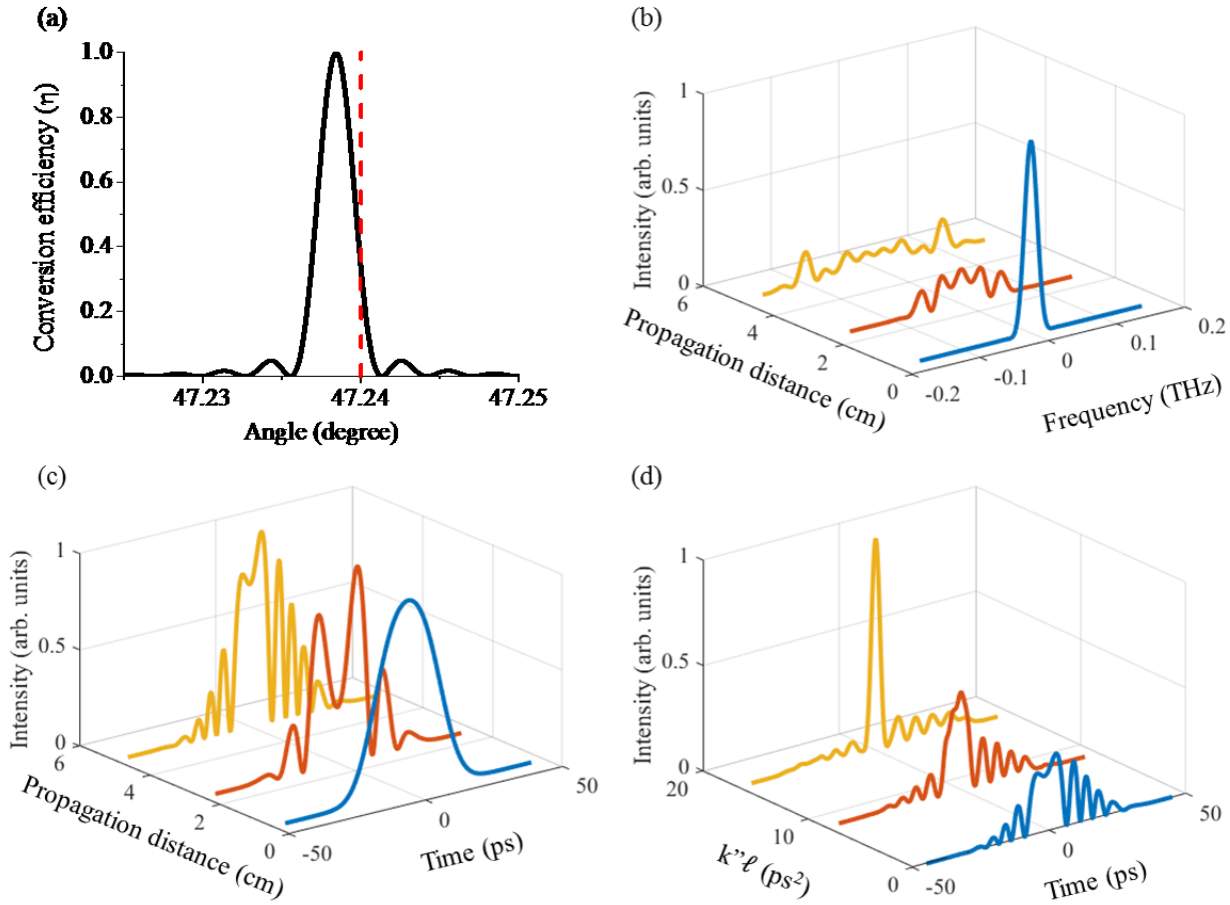

Figure 4: (a)Conversion efficiency for the sum frequency of two *cw* beams at 1064 nm and 532nm, as a function of the orientation of a 5cm KDP crystal. The dashed red line at 47.237 degree, corresponding to ($\Delta kL = 0.32\pi$) is chosen for the simulation in (b), where the sum frequency spectrum (centered at 355 nm) is plotted as function of propagation distance in a KDP crystal. In that case (b), two 25 ps pulses at 1064 and 532 nm are incident upon the crystal. (c) shows the same situation as (b) but plotted in the time domain. Figure (d) is again in the time domain, and shows the propagation of the 355 nm pulse extracted from the 5 cm KDP crystal in a linear element as a function of the dispersion of a transparent optical element.

to a stretcher at grazing incidence, where each grating has a groove density close to cut-off at the design wavelength (355 nm). Another possibility is to use a highly dispersive crystal (for instance $LiNbO_3$) which has a dispersion of 3340 fs^2/mm embedded in Gires-Tournois interferometer. With one face of a 5 cm crystal coated at 100% reflectivity, and the other with a reflectivity $\geq$ 96%, an enhancement of more than 100$\times$ of the material dispersion is achieved.

5 Application of cascaded nonlinearity for complete ultrashort pulse characterization

5.1 Overview of the temporal analysis methods available

Since the sub-picosecond time scale is beyond the reach of electronic instruments, purely optical methods had to be devised to reconstruct an ultrashort pulse in amplitude and phase. The first phase sensitive diagnostic method was the interferometric autocorrelation reported for the first time in 1978 [32]. Several methods based on the interferometric autocorrelation have been invented since to completely reconstruct a pulse in amplitude and phase. A combination of spectrum and interferometric autocorrelation provides enough phase and amplitude information to completely reconstruct a pulse in amplitude and phase [33, 34, 35]. The interferometric autocorrelation can be decomposed into its Fourier components to provide the needed information for spectral reconstruction [35]. The most intensely advertised reconstruction method is the frequency resolved optical gating or FROG, and its numerous derivatives [36]. The method requires a large number of iterations, and the commercial implementation has a limited dynamic range, as opposed to SPIDER [37] which requires hardly any iteration, and can be operated at high repetition rates.

It is shown in this section that cascaded nonlinearity can be exploited to create a single shot diagnostic method based solely on spectral measurements. A simple spectrometer provides the Fourier amplitude of an ultrashort pulse. Spectral phase information is required to reconstruct the pulse in the time domain. It has been shown that this phase information can be provided by an interferometric autocorrelation [38].

Based on the idea of using phase-carrying product SH and AC in MOSAIC, we are proposing an another method taking use of the cascading nonlinearity which will carry out the spectral phase with even simpler measurement that could be done with one spectrometer and two cascading SH crystals. Equivalently, the data required for temporal amplitude-phase reconstruction reduce to to a single shot autocorrelation, and two spectra (for the fundamental and second harmonic) [39].

5.2 Temporal reconstruction

It is shown here that the use of an autocorrelator is redundant, and the whole pulse temporal reconstruction in amplitude and phase can be achieved with spectral measurements, as sketched in Fig. 5. The measurements required are:

(a) The pulse spectrum

(b) The second harmonic spectrum

(c) The cascaded spectrum

The spectra (a) and (b) provide information on the spectral amplitudes, while (c) depends on the relative phase between fundamental and second harmonic.

With a second harmonic crystal in front of the spectrometer, as in Fig. 5(c), cross polarized fundamental and second harmonics are recorded. After grating dispersion, the spectrum of the fundamental and second harmonic (second order of grating dispersion) will overlap, giving a spectral intensity along an axis y (proportional to frequency):

$$I_1(y) \quad = \quad a|\mathcal{E}_1(\gamma\Omega)e^{i\phi_1(\gamma\Omega)}|^2 \tag{12}$$

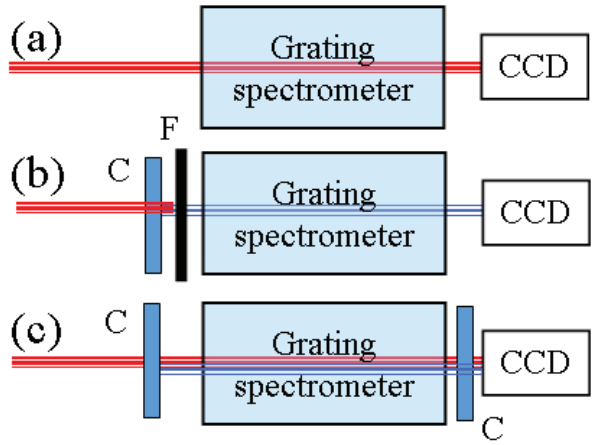

Figure 5: Basic sketch of the hardware required for reconstruction. While 3 spectrometers are shown for clarity, all measurements are to be performed with a single spectrometer. (a) Straight measurement of the pulse spectrum. (b) Measurement of the second harmonic of the pulse - a frequency doubling crystal (C) an a filter to eliminate the fundamental are inserted in front of the spectrometer. (c) "Cascade" measurement: The second harmonic and fundamental are sent together through the spectrometer; a second crystal is placed in front of the CCD detector.

$$I_2(y) \quad = \quad b|\mathcal{E}_2(\gamma\Omega/2)e^{i\phi_2(\gamma\Omega/2)}|^2. \tag{13}$$

γ is an instrument response factor converting the optical frequency into length in the spectrometer. The spectrum of the second harmonic in second order covers the same range as the spectrum of the fundamental in first order, hence the factor 1/2 in the expression for $I_2(y)$. Both of the spectra in Eqs. (12) and Eqs. (13) do not carry any phase information. However, the phase $\phi(y)$, which is the phase of a particular spectral component at y (hence the phase in the spectral domain), can be retrieved if a second nonlinear crystal phase matched again for frequency doubling is inserted in the spectrometer. At each coordinate y, depending on the phases $\phi_1(y)$ and $\phi_2(y)$, there will be energy transfer from/to the second harmonic to/from the fundamental, such that on the detector, the transmitted fields at Ω and 2Ω will be respectively:

$$\begin{aligned} \mathcal{E}_{s,\omega}(y) &= \mathcal{E}_1(y) + \chi^{(2)}\mathcal{E}_2(y)\mathcal{E}_1(y)e^{i(\phi_2-2\phi_1)}d \\ \mathcal{E}_{s,2\omega}(y) &= \mathcal{E}_2(y) - \chi^{(2)}\mathcal{E}_1(y)^2 e^{i(2\phi_1-\phi_2)}d \end{aligned} \tag{14}$$

where d is the second crystal length, assumed to be small. Within that approximation, the detected intensities $I_{s,b}$ and $I_{s,r}$ seen by the "blue" and "red" CCD sensors are:

$$\begin{aligned} I_{s,r}(y) &= a|\mathcal{E}_{s,\omega}(y)|^2 = |\mathcal{E}_1(y)|^2 + \left[\chi^{(2)}\mathcal{E}_2(y)\mathcal{E}_1^2(y)d\right]\cos(\phi_2 - 2\phi_1) \\ I_{s,b}(y) &= b|\mathcal{E}_{s,2\omega}(y)|^2 = |\mathcal{E}_2(y)|^2 - \left[\chi^{(2)}\mathcal{E}_1(y)^2\mathcal{E}_2(y)d\right]\cos(2\phi_1 - \phi_2) \end{aligned} \tag{15}$$

The three functions that can be used for a complete re-construction are now:

$$\begin{aligned} &I_1(y) \\ &I_2(y) \\ &\frac{I_{s,r}(y) - I_1(y)}{I_1(y)\sqrt{I_2(y)}} - \frac{I_{s,b}(y) - I_2(y)}{I_1(y)\sqrt{I_2(y)}} = 2\cos(2\phi_1 - \phi_2) \end{aligned} \tag{16}$$

In this proof-of-concept simulation, a complex spectral amplitude is expressed as $\tilde{\mathcal{E}}(\Delta\Omega) = \mathcal{E}(\Delta\Omega)\exp[i\phi(\Delta\Omega)]$. $\Delta\Omega$ is the spectral coordinate $\Delta\Omega = \Omega - \omega$, ω being the pulse central (average) frequency. For the pulse amplitudes, we chose the asymmetric pulse shape:

$$\mathcal{E}(\Delta\Omega) = \frac{2}{e^{a_1\Delta\Omega} + e^{-a_2\Delta\Omega}} \tag{17}$$

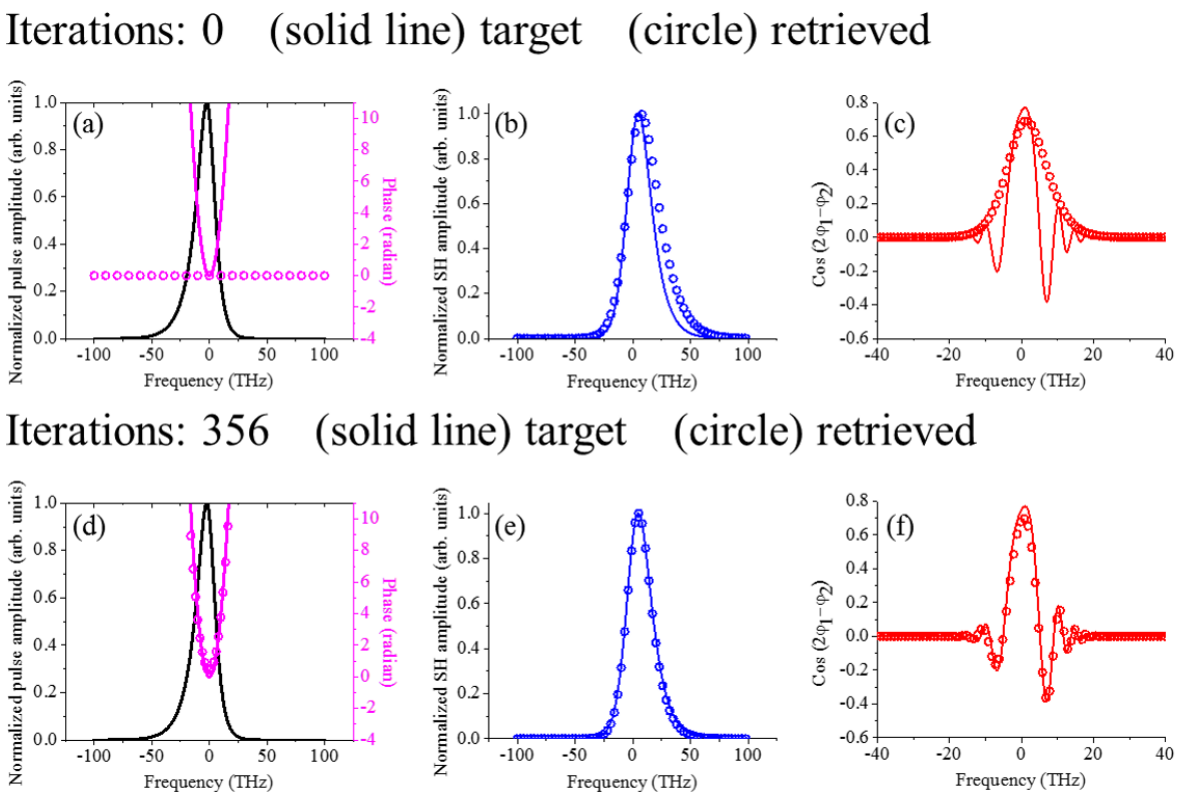

Figure 6: Spectral phase retrieval after 356 iterations. Pulse spectral phase is shown in solid magenta lines in (a,d), assigned with coefficients $\alpha = 40000fs^2$, $\beta = -50000fs^3$, and $\gamma = 60000fs^4$. The pulse rise and fall times are defined by the coefficients of the spectral envelope $a_1 = 200$ and $a_2 = 100$. The plots (a), (b) and (c) illustrate the first step of the spectral reconstruction, assuming zero spectral phase [magenta circle in (a)] and calculating the value of the error function using second harmonic (b) and cosine spectral phase difference $(2\varphi_1 - \varphi_2)$ (c) with Eq. 19. The algorithm then tries to minimize the error function. At number 356 iterations, apparent optimization can be seen in both second harmonic (e) and cosine spectral phase difference (f). In (d), the retrieved spectral phase $(2\varphi_1 - \varphi_2)$ (circles) is seen to match the initially assigned one (solid line).

For this particular demonstration, the phases are defined by the second, third and fourth order coefficients of a Taylor expansion of the spectral phase factor:

$$\phi = \alpha\Delta\Omega^2 + \beta\Delta\Omega^3 + \gamma\Delta\Omega^4 \tag{18}$$

As an example, α, β, and γ are set to be $40000fs^2$, -$50000fs^3$, and $60000fs^4$, and a_1 and a_2 are 200 and 100. Pulse spectrum with assigned coefficients is plotted in solid lines in Fig. 6(a), and SH and cosine spectral phase difference are plotted in solid lines in Fig. 6(b,c). The spectral phase retrieving process starts by assuming zero phase and to compute the profiles of SH and cosine phase difference as shown in circles in Fig. 6(a,b,c). The algorithm will try to minimize the error function Eq. 19 by changing α, β, and γ in sequence.

$$f_{error} = (I_{SH}^{assigned} - I_{SH}^{retrieved})^2 + (2\cos(2\phi_1^{assigned} - \phi_2^{assigned}) - 2\cos(2\phi_1^{retrieved} - \phi_2^{retrieved}))^2 \tag{19}$$

As shown in Fig. 6(d,e,f), optimum phase is found at number 356 iterations, assigned spectral phase(solid magenta) is well reproduced by the retrieved one (circle magenta).

6 Auto-stabilization of synchronously pumped Optical Parametric Oscillators

Simulation of quasi-phase-matching processes for ultrafast pulses in an intracavity pumped Optical Parametric Oscillator reveal an effective cross phase modulation which causes the coupling between OPO and pump cavities. This coupling can be exploited for auto-stabilization of an intracavity pumped OPO.

For the *coupled pump and OPO cavities*, a full numerical model is established by parameterizing the gain, loss, dispersion and nonlinearities. The pulse evolution of both pump laser and OPO is calculated at each cavity round trip. We use an ABCD matrix method in the temporal domain, inspired from the time-space analogy [40]. The simulation not only reproduces the observed instabilities, but leads to configurations where the signal and pump operations are stabilized in amplitude, phase and wavelength. The stable cavity uses counter-chirp in the pump and OPO cavities.

The model is based on the linear configuration of pump and OPO cavities sketched in Fig. 7. For the pump cavity, a pair of prism provides and adjustable dispersion, the (Ti:sapphire) gain and the saturable absorber (Multiple Quantum Wells of MQW) are modeled by rate equations. The OPO cavity contains only the periodically poled lithium niobate crystal (PPLN) of 1 mm thickness, and eventually a 5 mm long nonlinear crystal of lithium triborate (LBO) for creation of a tunable effective nonlinear index by phase mismatched second harmonic generation.

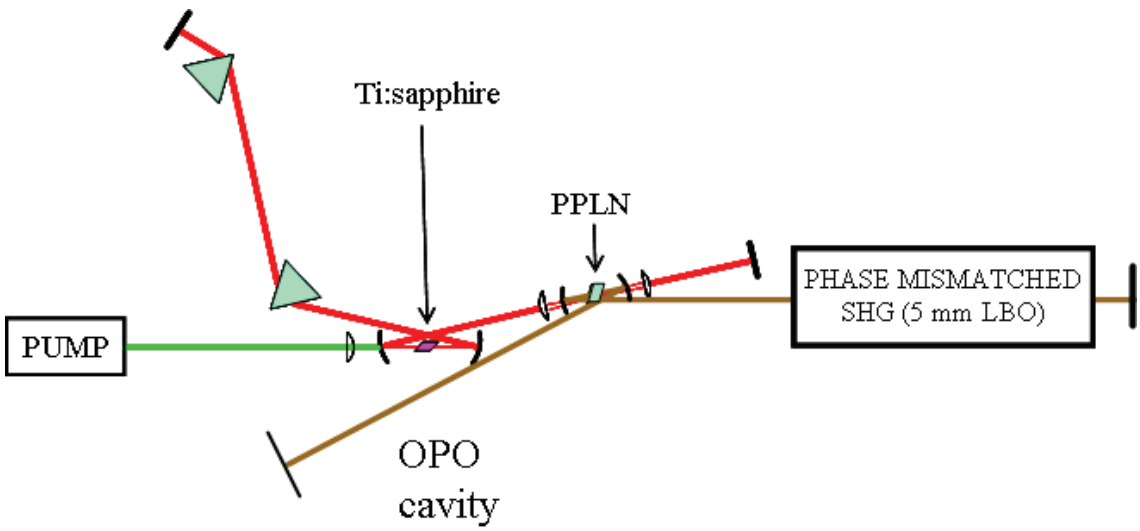

Figure 7: (a) Sketch of the OPO cavity, with a periodically poled crystal (PPLN) as a gain medium pumped intracavity by a Ti:sapphire mode-locked laser. Mode-locking is controlled by a Multiple Quantum Wells (MQW) saturable absorber and adjustable dispersion (pair of prisms).

6.1 Simulation of the coupled cavities

A pump pulse is circulating in the pump cavity, being amplified by a saturable gain, suffering linear attenuation at the mirrors and saturable absorbers MQW at the cavity end, and being reshaped through the coupling with the OPO signal in the PPLN crystal. The saturable media [gain and multiple quantum well (MQW) absorber] are modeled by two level systems [15]. The two level system parameters (gain cross section, upper level lifetime) were adjusted to match the results of a more elaborated four level system. The model was verified to be in agreement with the temporal evolution in the mode-locked Ti:sapphire.

The signal pulse is amplified and reshaped in its passage through the PPLN crystal, suffers linear and nonlinear losses in its cavity, and is reshaped again by passage through dispersive and Kerr elements. Previous simulation [41] computed the interaction and propagation through the nonlinear OPO crystal in 4 or 5 discrete steps, to evaluate the reshaping and gain taking place in the crystal. The signal and pump pulses temporal envelope was Fourier transformed to compute the effect of dispersion, then inverse Fourier transformed to compute the effect of nonlinearities (Kerr effect). The pulses were cycled for several thousand round-trips Practical limitations in computing time did not make it possible to compute the nonlinear interaction in the nonlinear crystal with more than 4 steps. As a result of this coarse stepping, some effects, such as cascaded nonlinearities, are not adequately accounted for. The present approach is to make a more detailed computation of the coupled propagation of various pulses through the nonlinear crystal. The 1 mm interaction distance is stepped in more than 100 steps, and a Butcher predictor-corrector method is used to solve numerically the set of differential equations (2) (in the frequency domain), providing the signal and pump output pulse shape (in amplitude and phase) for given input pulse shapes. A single propagation through the crystal takes about 90 minutes of computing time. It is not realistic to cycle this calculation (in addition to the propagation through other cavity elements) for thousands cavity round-trips. To gain in computing time by making a Gaussian beam approximation within the cavity. In this simplified approach, Gaussian temporal shapes with linear chirp are assumed. The general procedure is outlined by the sketch of Fig. 8. The pulses are characterized by their time of arrival at the crystal at each round-trip, their central frequency, pulse duration, chirp coefficient and energy. For a given set of Gaussian input pulse parameters (for the pump and signal, the propagation through the 1 mm thick PPLN crystal is computed. The results of this computation are fitted to a Gaussian, again characterized by a time delay through the crystal, a central frequency, pulse duration, chirp coefficient and energy. A large number of computation is performed to construct a matrix of output versus input parameters, representing the interaction within the crystal. Some example of the parametric dependence are presented in Section 2.1. In particular, it will be shown that the interaction of the fields in the OPO crystal can be approximated by nonlinear index if refraction creating chirp in the pump and OPO cavities. This nonlinear index of refraction changes from one round-trip to the next, with changes in pulse intensity. To model effectively the pulse dynamics in each cavity due to self phase modulation and dispersion, we use a paraxial-time approximation to circulate the pulses through successive dispersion and Kerr phase modulation. A time matrix approach — similar to the method used in Gaussian beam propagation — is introduced.

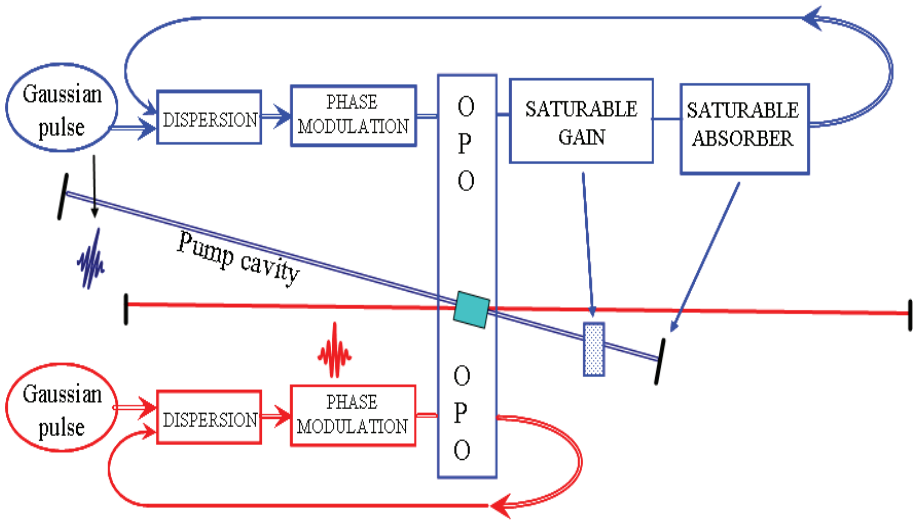

Figure 8: Model for the numerical simulation of the cavity. All pulses are assimilated to Gaussian pulses characterized by their duration, energy, linear chirp and time of arrival.

6.2 Parametric modeling of the interaction in the OPO crystal

A pair of Gaussian pump pulse and signal pulse are sent into a 1 mm thick periodically poled crystal, characterized by its period of 20.23 μm. The input parameters are the pulse durations, chirp, central wavelength, energy, and delay of the signal with respect to the pump pulse. The Eqs. (2) are solved numerically to calculate the transmitted pulses, resulting from the various mixing processes indicated in Fig. 1. The output pulses are in turn approximated by Gaussian. Sets of output pulse parameters are tabulated, for various sets of input parameters. Input pulses are 100 fs, 300 μJ/cm^2 pump pulse at 770 nm co-propagating with 100 fs, 200 μJ/cm^2 signal pulses at 1140 nm.

6.2.1 OPO Gain — dependence on timing

The group velocity of the signal is much larger than that of the pump, which is the reason for using only a 1 mm long PPLN crystal. Indeed, these pulses experience a temporal walk off of 233 fs after propagation through 1 mm of $LiNbO_3$, a walk-off that is larger than the pulse duration. The signal gain and pump depletion are function of the initial delay of the signal with respect to the pump, which is plotted in Fig. 9. This plot illustrates that the delay between pump and signal pulses is an important parameter.

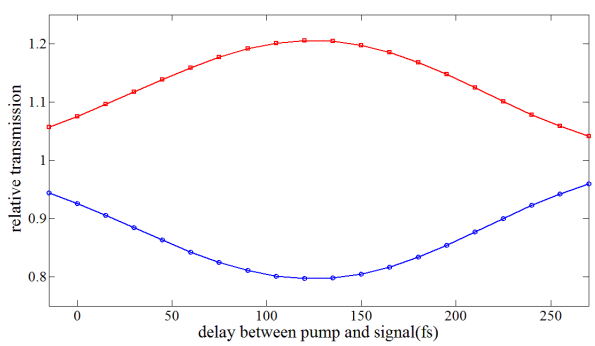

Figure 9: Transmission of pump and signal pulse energy after propagation through a 1mm PPLN for different time delays between them. Red stands for pump, blue for signal. The delay time is varied from -15fs to 270fs, in 15fs interval. The maximum conversion is achieved around 120fs.

6.2.2 Chirp Generation

Calculation of the non-phase matched processes shows that a phase modulation is imparted onto the pump pulse. An example is shown as Fig. 10(a), where the phase of the pump (solid line) and the phase of the signal (dashed line) are plotted as a function of intensity, for a signal 10 nm off from phase matching condition. As generally observed, the "cross phase modulation", phase of pump field versus signal intensity, is much larger than the "self phase modulation" (phase of signal field versus signal intensity). The nearly linear phase dependence on intensity can be approximated by a (negative) nonlinear index of refraction.

These two nonlinear indices induced by near resonant DFG have a wavelength dependence which is linear within 15 nm of the phase-matched wavelength as shown in Fig. 10(b), and can be approximated by:

$$n_{2,ps} = \frac{(1140 - \lambda_s)}{39} \cdot 10^{-14}\text{cm}^2/\text{W} \tag{20}$$

$$n_{2,sp} = \frac{(1140 - \lambda_s)}{108} \cdot 10^{-14}\text{cm}^2/\text{W} \tag{21}$$

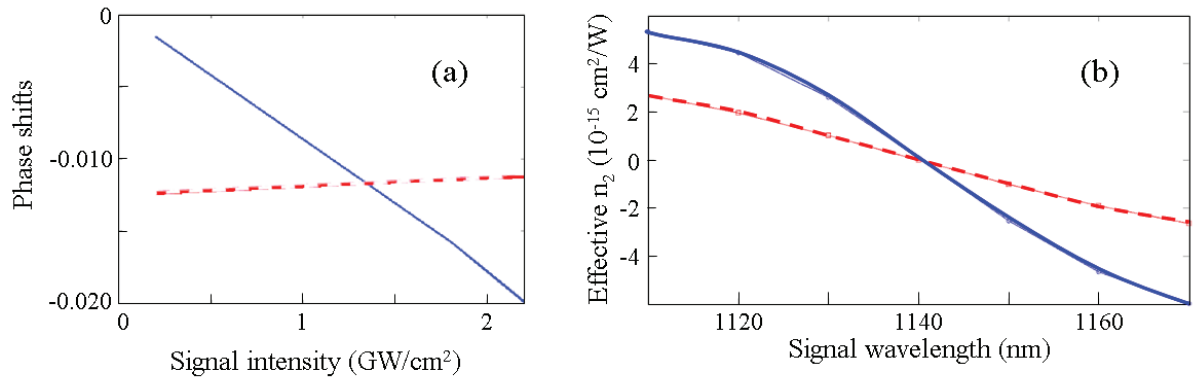

Figure 10: (a) Phase shift versus intensity of the signal pulse, for the pump field (solid line) and the signal field (dashed line). The signal wavelength is detuned by 10 nm with respect to the perfect quasi-phase matching condition. (b) Effective n_2 of pump (blue) and signal (dashed red) as a function of signal wavelength.

The first nonlinear index $n_{2,ps}$ causes a nonlinear phase shift for the pump, proportional to the signal intensity, and the second nonlinear index $n_{2,sp}$ produces a nonlinear phase shift for the signal, proportional to the pump intensity. 1140 nm is the quasi-resonant wavelength of quasi-phase matching for the pump wavelength of 770 nm. These results demonstrate the important impact of the often neglected phase-mismatched processes on the interaction of pump and signal pulses in an OPO crystal.

There are other, smaller but non negligible, contributions to the nonlinear index, from non-phase matched sum frequency generation processes. Calculation of the non-phase matched processes show that a phase modulation is imparted onto the pump pulse, To the second harmonic generation process of the pump is associated a nonlinear index $n_{2,p} = -1.1 \times 10^{-16}$ cm^2/W. Another contribution to the phase modulation of the pump is the sum frequency generation process $\omega_p + \omega_s$, to which can be associated a nonlinear index $n_{2,p} = -1.9 \times 10^{-16}$ cm^2/W. The latter process in turn imparts a phase modulation on the signal pulse that can be represented by an effective nonlinear index $n_{2,s} = -1.2 \times 10^{-16}$ cm^2/W.

6.2.3 Delay dependence of the wavelength

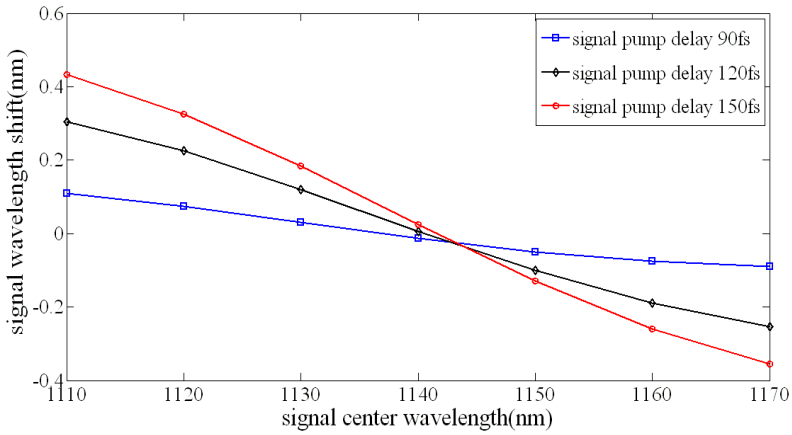

Figure 11: Wavelength shift for signal pulse after propagation in a 1mm PPLN as a function of signal wavelength for different delay time 90fs (blue), 120fs (black) and 150fs (red).

The spectrum of signal pulse can be shifted by the nonlinear interaction. The shift of the center of gravity of the signal spectrum is computed as a function of the delay between signal and pump. This wavelength shift is less than 0.1% of the signal spectrum, but can be non negligible when the signal pulse propagates many round trips in the OPO cavity. This wavelength shift is plotted in Fig. 11 for different signal wavelength and input delays of 90fs, 120fs and 150fs respectively. The various curves cross at the same wavelength of quasi phase-matching, indicating that this is a preferred wavelength, but without any indication on whether it will lead to a stable operating point in the OPO cavity. n fact the cavity becomes unstable if one wants to tune the OPO away from the preferred wavelength (1140nm in this case). Therefore other parameters for instance chirp is introduced to modify the wavelength shift as a function of delay. The signs and values of chirp for pump and signal wavelength are carefully chosen in Sectionwave-change-OPO

6.3 Circulation of Gaussian pulses in a cavity

The dispersive properties of the cavity are lumped into a second order dispersion/round-trip, and a Kerr modulation. For the pump cavity, the dispersion has a fixed (positive) contribution from the PPLN and gain crystals, and a negative contribution (adjustable) from a pair of prisms [42]. The Kerr effect has a contribution from the Ti:sapphire gain crystal, the PPLN crystal, and the phase mismatched interactions parametrized in the previous section. The OPO cavity dispersion is dominated by that of the PPLN crystal. The Kerr modulation includes the material n_2 from the PPLN, the contribution from the phase mismatched processes computed in the previous section, and an adjustable positive or negative contribution from a phase mismatched nonlinear crystal inserted in the OPO cavity (see Fig. 7). It is shown in this section that the (temporal) dispersive properties of the cavity can be calculated at each round-trip by simple products of 2 $\times$ 2 matrices, the time analogue of the ABCD matrices used for Gaussian beam propagation.

6.3.1 Space-time analogy for Gaussian beams/pulses

Item	Space element	Time element
Gaussian	$\tilde{\mathcal{E}} = \mathcal{E}_0 \frac{w_0}{w} e^{-r^2/w^2} e^{-ir^2/2R}$ $w = 1/e$ radius of field R a phasefront curvature	$\tilde{\mathcal{E}} = \mathcal{E}_0 \frac{\tau_{g0}}{\tau_G} e^{-t^2/\tau_g^2} e^{-i\ddot{\varphi}t^2/2}$ $\tau_g = 1/e$ halfwith of envelope $-i\ddot{\varphi}t^2/2$ = quadratic temporal phase modulation
beam / pulse parameter	$\frac{1}{q} = \frac{1}{R} - i\frac{\lambda}{\pi w^2}$ $\lambda = \lambda_0/n$, R=curvature	$\frac{1}{p} = \ddot{\varphi} - \frac{2i}{\tau_g^2}$ $\ddot{\varphi} = \partial^2\varphi/\partial t^2$
diffraction/dispersion	$\begin{matrix} 1 & d \\ 0 & 1 \end{matrix}$	$\begin{pmatrix} 1 & \psi'' \\ 0 & 1 \end{pmatrix}$
Element	d	$\frac{d^2\psi}{d\Omega^2}$
focusing matrix Element	$\begin{pmatrix} 1 & 0 \\ -\frac{1}{f} & 1 \end{pmatrix}$ f=focal length	$\begin{pmatrix} 1 & 0 \\ c_t & 1 \end{pmatrix}$ $c_t = \frac{8\sqrt{2\pi}\ell_{Kerr}}{\lambda_0} n_2 \frac{W}{\tau_g^3} = \frac{T_c}{\tau_g^3}$
Plane-curve $ABCD$	$\begin{pmatrix} 1-\frac{d}{f} & d(2-\frac{d}{f}) \\ -\frac{1}{f} & 1-\frac{d}{f} \end{pmatrix}$	$\begin{pmatrix} 1+\psi''c_t & \psi''(2+\psi''c_t) \\ c_t & 1+\psi''c_t \end{pmatrix}$
waist/shortest limit $\to 0$	$w_0^2 = \frac{\lambda}{\pi}\sqrt{d(2f-d)}$ $d = 2f$ and $w_0 \to 0$	$\tau_{G0}^2 = 2\sqrt{-\psi''(\frac{2}{c_t} + \psi'')}$ $\tau_{g0} \approx 2\left(\frac{2\psi''^2}{T_c}\right)^{1/3}$

Table 1: Comparative table of space and time matrices. Note the representation of the Kerr phase modulation c_t as the ratio of a physical time constant T_c and the cube of the pulse duration.

The beam parameters in a laser cavity are set by the focal distances of lenses and mirrors, and diffraction.

A modeling of the beam characteristics in the cavity can be made using paraxial approximation, where the Gaussian beam is characterized by a "q" parameter that depends on the wavelength, the beam $1/e^2$ radius w and the wavefront curvature R. All optical elements are represented by a 2 by 2 matrix (ABCD matrix) [43], that can successively operate on the beam. A time-space analogy [40] allows to transpose the Gaussian beam formalism to the time domain, using a similar matrix representation. The pulse parameter "p" is defined by its pulse width "τ_g" and a quadratic phase curvature $\ddot{\varphi} = \partial^2\varphi/\partial t^2$. Similarly as the space $ABCD$ matrix acts on the q parameter as $q_2 = (Aq_1 + B)/(Cq_1 + D)$, the time $ABCD$ matrix acts on the p parameter as $p_2 = (Ap_1 + B)/(Cp_1 + D)$ Paraxial approximation for the optical pulses refers to having a small dynamics in pulse duration (narrow distribution in time). The comparison between time and space beam parameters and optical elements are given in table 1.

There are a few important differences to note between space and time. Diffraction can only be positive as a beam expands in space. Dispersion can be positive or negative, depending on the sign of $\psi'' = d^2\psi/d\Omega^2$, where $\psi(\Omega)$ is the spectral phase shift imposed on the field by a particular optical element. Another important difference is that the focal distance — in space — is solely determined by the geometry of a lens or mirror. In time, the parabolic phase is determined by the Kerr effect, and its curvature c_t is therefore inversely proportional to the cube of the pulse duration τ_g. It is interesting to compare the plane-curved mirror cavity (last to lines of table 6.3) in space and time. In the half concentric limit of $d \to 2f$, the beam wasit in space can be arbitrarily small. In time however, there is a minimum pulse duration at the "*waist*" set by the ratio of dispersion to Kerr effect.

6.4 Complete cavity simulation

Given a set of initial condition, the pump and OPO pulses are cycled in the cavity using the procedure outlined in Fig. 8. The result reproduce the unstable patterns observed experimentally, and are therefore of little interest. One of the essential source of instability stems from cavity length fluctuations, exacerbated by the fact that the pulses are very short and the cavity very long. The discussion that follows points to a self-stabilizing mechanism that can modify the OPO wavelength in a manner as to preserve synchronism between cavities. The numerical simulation confirm that indeed this procedure leads to stable operation of the mode-locked pump and OPO.

6.4.1 Wavelength changes induced in the OPO

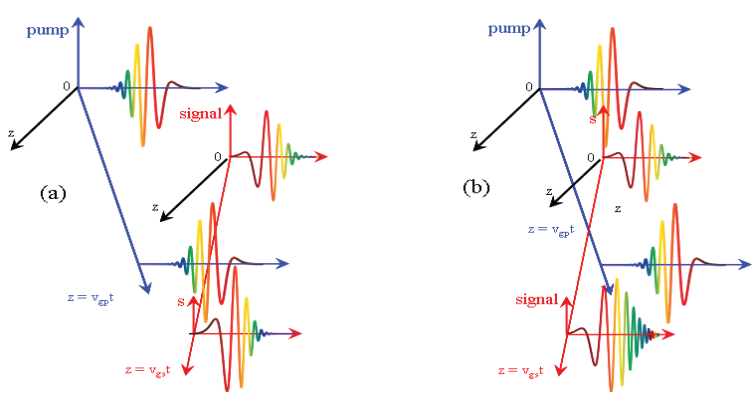

Figure 12: (a) Because of an elongation of the OPO cavity, the pump pulse is already in the middle of the PPLN crystal when the OPO pulse is just entering. The pump and signal pulses only interact over their lowest frequencies, resulting in a shift of the average signal wavelength towards longer values. With the positive dispersion in that cavity, the signal pulse will accelerate, compensating the initial delay.

It is an accepted concept that an externally synchronously pumped OPO changes wavelength to track the repetition rate of the pump. There are however two different mechanisms that can account for this apparent tracking.

1. If the repetition rate of the pump is modified, the OPO is no longer at synchronism, and the oscillation ceases. The laser starts again from noise, and the wavelength components that match the pump period through their group velocity emerge.
2. There is a real wavelength shift at each passage through the OPO if the repetition rates is not matched.

In the first case, the laser will show maximum instability, since the wave has to die and be resuscitated at each cavity length fluctuation.

The second mechanism, if it exists and can be enhanced, may be the key to intracavity pumped OPO stabilization. In order to achieve self-stabilizing operation, a counter-chirped pump and signal pulse model is proposed. Figure 12 is an illustration of this concept, for the case of a pump cavity with negative dispersion, a downchirped pump pulse, and an OPO cavity with positive dispersion, and an upchirped signal.

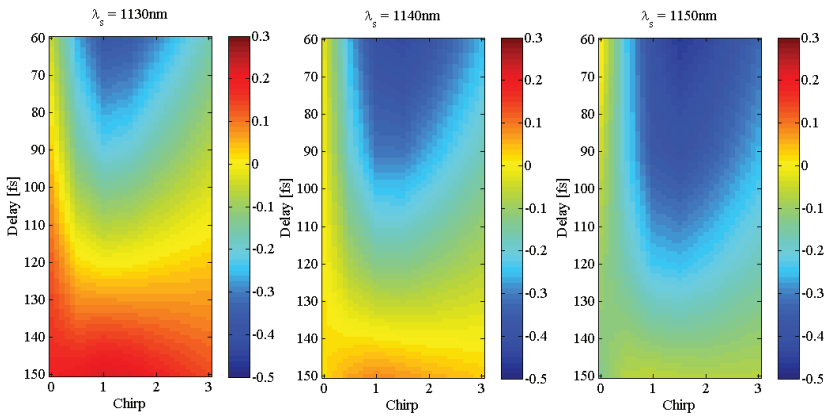

Figure 13: Wavelength shift for signal pulse after propagation in a 1mm PPLN for different wavelength (1130 to 1150nm), delay (60 to 150fs) and chirp coefficient (0 to 3)

The signal having a larger group velocity than the pump, optimum overlap of pump and signal in the OPO crystal requires that the signal be delayed with respect to the pump at each passage. Let us imagine an equilibrium situation in which the cavities are at synchronism, with the signal having an optimum advance over the pump. In the situation depicted in Fig. 12, the OPO cavity is given a sudden expansion, resulting in an additional delay of the signal in the crystal. The pump is well in advance of the signal when the latter enters the crystal [Fig. 12 (a)]. The signal barely catches up with the pump at the end of the crystal [Fig. 12 (b)], resulting in amplification of the lower frequencies of the signal. With the average signal frequency down-shifted in the cavity with positive dispersion, the signal delay will decrease. While the majority of material nonlinear index n2 is positive, we can control the sign and value of effective nonlinear index through cascade nonlinear interactions, such as phase mismatched second harmonic generation.

Wavelength shifts in the PPLN crystal

The propagation of the OPO signal through the PPLN crystal is computed for signal wavelengths of 1130, 1140 and 1150nm, and delay time (with respect to the pump pulses) of 60, 90, 120 and 150fs, The chirp coefficients are 0.5, 1, 1.5, 2 and 3. A linear interpolation for the 3D wavelength shifts data (Fig. 13) is performed afterwards. Figure 13 shows that the wavelength shift is indeed magnified with chirp as compared

to the shift calculated for unchirped pulses (See Fig. 11. The maximum effect is reached for a chirp coefficient around 1.5.

6.4.2 Demonstration of autostabilization

Step function response of the cavity In each round trip, the 100 fs, 30 nJ pump pulse centered at 770 nm interacts with a 100 fs, 3 nJ signal pulse centered at 1140 nm in a PPLN crystal of 1 mm long, period 20.23μm. Thereafter the pump and signal pulses experience gain/loss, dispersion/nonlinearity in their own cavities, respectively. The pulse energy, pulse duration and chirp are examined at each cavity round trip. The delay between signal and pump pulses is another important parameter as it is used in the simulation to determines the synchronization of Ti:Saph and OPO cavities. Mostly importantly we examine the signal wavelength evolution as a function of cavity round trips, because we are particularly interested in the signal wavelength shifts that tracks the OPO cavity detuning with respect to the Ti:Sapphire cavity.

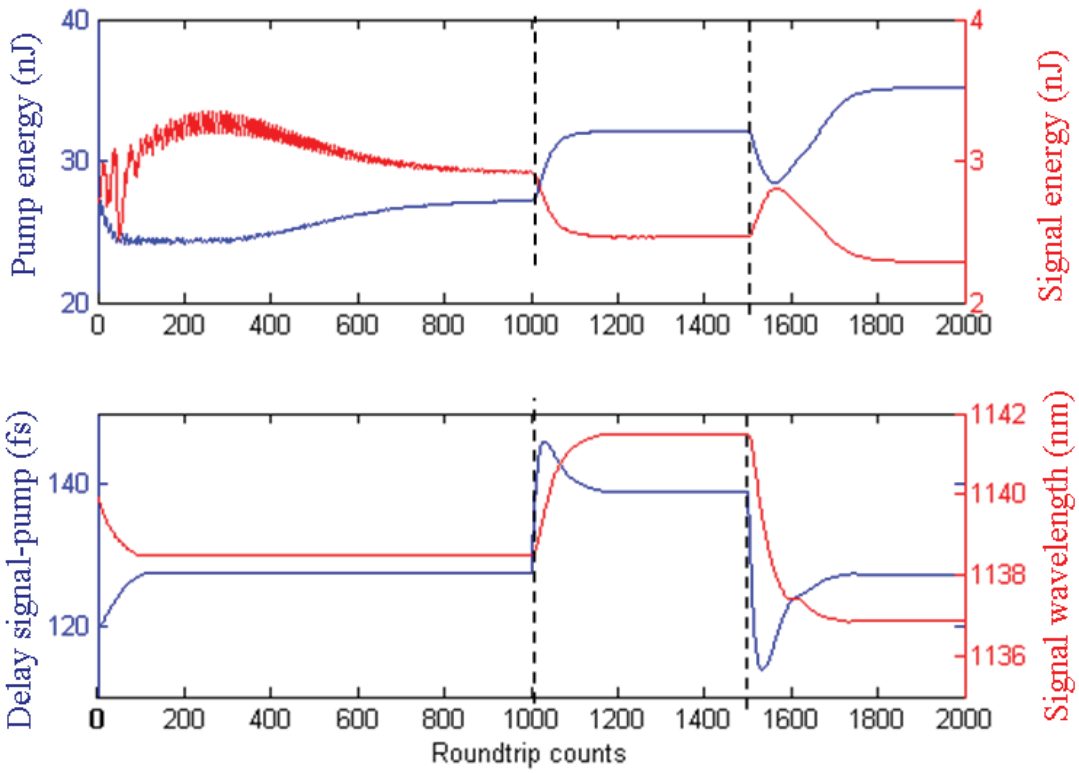

Figure 14: GVD=-1600fs^2 (pump), 1000 fs^2 (signal); Linear loss =11% (pump), 7% (signal); OPO gain = 1.15-0.5$\times E_s$; Pump depletion = 0.91-0.1 $\times E_s$; Non linear loss coefficient = $1.5 \cdot 10^6$; Damping coefficient = 0; Initial λ_s = 1140nm. A sudden change of 1.7fs (longer signal cavity) is applied to the signal pulse at each round-trip, starting after 1000 round-trips (first dashed line). A sudden shortening of the signal cavity is applied after 1500 round-trips, which results in an advance of -2.2 fs of the signal pulse. In both cases, the wavelength of the signal changes as to reach a new equilibrium.

The signal wavelength of a synchronously pumped OPO is known to be determined by the cavity length of the OPO within the gain bandwidth. The simulation of Fig. 14 shows that the signal wavelength will vary in the range of 5 nm, for sudden cavity length changes in the range of 700 nm. Once the pulse parameters have

reached equilibrium (at round-trip index 1000 in Fig. 14, a 1.7 fs change in signal delay is applied at every round-trip. A new set of equilibrium parameters is reached after some transients. The signal wavelength increases, and at the increased group velocity the signal reaches again synchronism with the pump. At round-trip index of 1,500, a second jump of -2.2 fs brings a new stable condition at a shorter wavelength. The wavelength tunes itself continuously to track synchronism with the pump.

7 Conclusion

The main conclusion of this work is that dispersion and phase matching bandwidth do not set a fundamental limit to type II pulse compression in sum-frequency generation as long as they are used in a controlled fashion. Amplitude modulation through fast depletion of the fundamental pulses provides the extra bandwidth required to generate ultrashort pulses. We have presented a theoretical model sufficient to describe the desired effects, pointed out its limitations and have compared it to existing models which do not use the full dispersion dependence. The model has been applied to compression of 14 ps to 310 fs pulses and has also been experimentally verified. Furthermore, compression of 10 fs ultrashort pulses down to 2.5 fs in the second-harmonic as well as fundamental wavelength has been predicted. In the ultrashort pulse case, the experimental requirements are rather modest, since a relatively long crystal can be used, and the energy tilt requires only a small angle prism. We have chosen to illustrate the method by specific calculations applied to second harmonic generation of 800 nm pulses in BBO. However, it can be applied to frequency mixing in various crystals. The same approach can also be applied to parametric generation, extending the compression method demonstrated by Umbrasas *et al.* [6]. In this work we exploit the properties of group velocity dispersion at the various wavelengths to achieve the desired compression, rather than to select a particular orientation of a particular crystal (BBO) that has near-zero dispersion [44]. The latter technique leads to impressive results, but is limited to amplification and generation of wavelengths longer than 560 nm.

One other examples of application of the model that are covered in this chapter is the creation of a giant bandwidth for compression of ps pulses. Even though dramatic pulse splitting occurs in this process, it is shown that the multiple split pulses spread over 25 ps can be rejoined in a 3.5 ps pulse.

The numerical model is also applied to pulse diagnostic, and a new method of pulse reconstruction is presented based on cascaded nonlinearity in a spectrometer. Related to pulse diagnostic, contrary to a widely held misconception [36], it is shown that considerably longer (thicker) second harmonic crystals can be used for intensity autocorrelation of fs pulses, than the thickness required to have overlapping fundamental and second harmonic through the crystal [36], or the pulse longer than the inverse phase matching bandwidth.

The theoretical model applies to difference frequency generation: it is shown that the use of counter-chirped pump and signal pulses can act on the group velocities in order, for instance, to stabilize optical parametric oscillators.

References

[1] Y. Wang and R. Dragila. Efficient conversion of picosecond laser pulses into second-harmonic frequency using group-velocity-dispersion. *Phys. Rev. A*, 41:5645–5649, 1990.

[2] A. Stabinis, G. Valiulis, and E. A. Ibragimov. Effective sum frequency pulse compression in nonlinear crystals. *Optics Comm.*, 86:301–306, 1991.

[3] Y. Wang and B. Luther Davies. Frequency-doubling pulse compressor for picosecond high power neodymium laser pulses. *Opt. Lett.*, 17:1459–1461, 1992.

[4] P. Heinz, A. Laubereau, A. Dubietis, and A. Piskarskas. Fiberless two-step parametric compression of sub-picosecond laser pulses. *Lithuanian Phys. Rev.*, 33:314–317, 1993.

[5] A. Umbrasas, J. C. Diels, G. Valiulis, J. Jacob, and A. Piskarskas. Generation of femtosecond pulses through second harmonic compression of the output of a Nd:YAG laser. *Opt. Lett.*, 20:2228–2230, 1995.

[6] A. Umbrasas, J. C. Diels, J. Jacob, and A. Piskarskas. Parametric oscillation and compression in KTP crystals. *Opt. Lett.*, 19:1753–1755, 1994.

[7] J. D. V. Khaydarov, J. H. Andrews, and K. D. Singer. Pulse compression in a synchronously pumped optical parametric oscillator from group-velocity mismatch. *Opt. Lett.*, 19:831–833, 1994.

[8] J. D. V. Khaydarov, J. H. Andrews, and K. D. Singer. 20-fold pulse compression in a synchronously pumped optical parametric oscillator. *Appl. Phys. Lett.*, 65:1614–1616, 1994.

[9] L. Lefort, S.D. Butterworth, Y.P. Svirko, K. Puech, D. C. Hanna, and D.H. Jundt. Generation of fs pulses from order of magnitude pulse compression in a cw synchronously pumped optical parametric oscillator. In *CLEO '98, San Francisco, USA*. OSA, 1998.

[10] Robert W. Boyd. *Nonlinear optics*. Academic Press, third edition, 2008.

[11] Y. R. Shen. *The Principles of Nonlinear Optics*. John Wiley & Sons, New York, 1984.

[12] Jens Biegert, Vaclav Kubecek, and Jean-Claude Diels. Pulse compression: Type II second harmonic pulse compression. In John G. Webster, editor, *Encyclopedia of Electrical and Electronics Engineering (#17)*, volume 17, pages 446–454. IEEE, 1998.

[13] J. Biegert and J. C. Diels. Compression of pulses of a few optical cycles through harmonic conversion. *Journal of Optical Society B*, 18:1218–1226, 2001.

[14] J. C. Butcher. *Numerical methods*. 1960.

[15] J.-C. Diels and Wolfgang Rudolph. *Ultrashort laser pulse phenomena*. Elsevier, ISBN 0-12-215492-4; second edition, Boston, 2006.

[16] Xuan Luo. *Investigation of intracavity phase interferometry applied to femto-metrology*. PhD thesis, The University of New Mexico, Albuquerque,New Mexico, 2014.

[17] L. Arissianr. High intensity laser physics, filamentation, air lasing. Invited presentation at the joint joint workshop on Defence Applications of Quantum 2.0 Phenomena, 2017.

[18] Ladan Arissian and Jean-Claude Diels. *Mode-locked lasers*. Elsevier, 2017.

[19] Xiaozhen Xu, Chengyong Feng, and Jean-Claude Diels. Optimizing sub-ns pulse compression for high energy application. *Optics Express*, 22:13904–13915, 2014.

[20] Chengyong Feng, Jean-Claude Diels, and Xiaozhen Xu. Spatiotemporal characterization of pulses obtained from a high-energy sub-nanosecond laser system. *Applied Optics*, 55:1603–16012, 2016.

[21] Chengyong Feng, Xiaozhen Xu, and Jean-Claude Diels. High-energy sub-phonon lifetime pulse compression based on stimulated Brillouin scattering in liquids. *Submitted to J. Phys. B: atomic and molecular optics.*, 2017.

[22] Koji Masuda, James Hendrie, Jean-Claude Diels, and Ladan Arissian. Envelope, group and phase velocities in a nested frequency comb. *Journal of Physics B*, 49:085402, 2016.

[23] James Hendrie, Matthias Lenzner, Hanieh Akhamiardakani, Jean-Claude Diels, and Ladan Arissian. Impact of resonant dispersion on the sensitivity of intracavity phase interferometry and laser gyros. *Optics Express*, 24:30402–304010, 2016.

[24] W. Koechner and M. Bass. *Solid-State Lasers*. Springer, ISBN 3-387-95590-9, Berlin, Heidelberg, New York, 2002.

[25] Jens Biegert, Vaclav Kubecek, and Jean-Claude Diels. Second harmonic pulse compression. In *Ultrafast Phenomena XI*, pages 84–86. Springer-Verlag, 1998.

[26] Yu-Chen Cheng, Chih-Hsuan Lu, Yuan-Yao Lin, and A. H. Kung. Supercontinuum generation in a multi-plate medium. *Opt. Express*, 24(7):7224–7231, Apr 2016.

[27] Chih-Hsuan Lu, Yu-Jung Tsou, Hong-Yu Chen, Bo-Han Chen, Yu-Chen Cheng, Shang-Da Yang, Ming-Chang Chen, Chia-Chen Hsu, and A. H. Kung. Generation of intense supercontinuum in condensed media. *Optica*, 1(6):400–406, Dec 2014.

[28] H. J. Bakker, P. C. M. Planken, L. Kuipers, and A. Lagendijk. Phase modulation in second-order nonlinear-optical processes. *Phys. Rev. A*, 42:4085–4101, Oct 1990.

[29] P. C. M. Planken, H. J. Bakker, L. Kuipers, and A. Lagendijk. Frequency chirp in optical parametric amplification with large phase mismatch in noncentrosymmetric crystals. *J. Opt. Soc. Am. B*, 7(11):2150–2154, Nov 1990.

[30] Richard DeSalvo, David J. Hagan, G. Stegeman, and Eric W. Van Stryland. Self-focusing and self-defocusing by cascaded second-order effects in KTP. *Optics Letters*, 17:28–30, 1993.

[31] Guoqiang Xie, Dongfang Zhang, Liejia Qian, Heyuan Zhu, and Dingyuan Tang. Multi-stage pulse compression by use of cascaded quadratic nonlinearity. *Optics Communications*, 273(1):207 – 213, 2007.

[32] J.-C. Diels, E. W. Van Stryland, and G. Benedict. Generation and measurements of pulses of 0.2 psec duration. *Opt. Comm.*, 25:93, 1978.

[33] J.-C. Diels, J. J. Fontaine, I. C. McMichael, and F. Simoni. Control and measurement of ultrashort pulse shapes (in amplitude and phase) with femtosecond accuracy. *Applied Optics*, 24:1270–1282, 1985.

[34] K. Naganuma, K. Mogi, and H. Yamada. General method for ultrashort light pulse chirp measurement. *IEEE J. of Quantum Electronics*, QE-25:1225–1233, 1989.

[35] Chi Yan and J.-C. Diels. Amplitude and phase recording of ultrashort pulses. *J. of the Opt. Soc. Am. B*, 8:1259–1263, 1991.

[36] R. Trebino. *Frequency-Resolved Optical Gating, The Measurement of Ultrashort Laser Pulses*. Kluwer, 2002.

[37] C. Iaconis, V. Wong, and I. A. Walmsley. Direct interferometric techniques for characterizing ultrashort optical pulses. *IEEE Selected Topics in Quant. Electron.*, 4(2):285–294, 1998.

[38] D. A. Bender and M. Sheik-Bahae. Modified spectrum autointerferometric correlation (mosaic) for single-shot pulse characterization. *Optics Letters*, 32:2822–2824, 2007.

[39] Ning Hsu and J.-C. Diels. High dynamic range single shot diagnostic of ultrashort pulses applied to optical parametric oscillator. In *Photonics West, SPIE-LASE*, volume 10089, pages 10089–25, San Francisco, CA, 2017. SPIE.

[40] B. H. Kolner and M. Nazarathy. Temporal imaging with a time lens. *Optics Lett.*, 14:630–632, 1989.

[41] Andreas Velten, Andreas Schmitt-Sody, and Jean-Claude Diels. Precise intracavity phase measurement in an optical parametric oscillator with two pulses per cavity round-trip. *Optics Letters*, 35:1181–1183, 2010.

[42] Ladan Arissian and Jean-Claude Diels. Carrier to envelope and dispersion control in a cavity with prism pairs. *Physical Review A*, 75:013814–013824, 2007.

[43] H. W. Kogelnik and T. Li. Laser beams and resonators. *Appl. Opt.*, 5:1550–1567, 1966.

[44] A. Shirakawa, I. Sakane, M. Takasaka, and T. Kobayashi. Sub-5-fs pulse generation by pulse-front-matched noncollinear optical parametric ampli
cation. *Appl. Phys. Lett.*, 74:2268, 1999.